

Article

Optimal SOC Control and Rule-Based Energy Management Strategy for Fuel-Cell-Based Hybrid Vessel including Batteries and Supercapacitors

Zeyu Ma ¹, Hao Chen ^{1,*} , Jingang Han ¹ , Yizheng Chen ¹, Jiongchen Kuang ¹, Jean-Frédéric Charpentier ² , Nadia Ait-Ahmed ³  and Mohamed Benbouzid ^{1,4} 

¹ The Research Institute of Power Drive and Control, Shanghai Maritime University, Shanghai 201306, China

² Institut de Recherche de l'École Navale (EA 3634 IRENav), French Naval Academy, 29240 Brest, France

³ Institut de Recherche en Energie Electrique de Nantes Atlantique, Nantes University, 44602 Saint-Nazaire, France

⁴ Institut de Recherche Dupuy de Lôme (UMR CNRS 6027 IRDL), University of Brest, 29240 Brest, France

* Correspondence: chen hao@shmtu.edu.cn

Abstract: Around the world, the development of electric vehicles is underway, including in maritime transportation. However, the development of clean energy vessels still has a long way to go. Fuel cells (FCs) are a relevant choice among the many clean energy sources to power clean energy vessels. However, due to the complex and drastic change in the shipload power, FCs need to be equipped with dynamic fast-response energy storage equipment to make up for it. For multiple energy storage devices connected in parallel, the state of charge (SOC) is not balanced, which affects their service life and the stability of the vessel microgrid, as well as slowing the speed and lowering the accuracy of SOC equalization. This paper proposes a distributed variable sag slope control strategy for vessels to improve SOC equalization, with a FC as the energy source and a battery and supercapacitor as the energy storage system (ESS). For the output power distribution problem of energy storage equipment caused by shipload power variation, a power distribution strategy with a variable filter time constant is used to improve the reasonableness of the output power distribution of energy-based lithium batteries and power-based supercapacitors. Meanwhile, this paper considers the power generation equipment's service life and energy cost as the optimization objectives, considering the discharge depth of the energy storage equipment. Finally, a method based on the combination of the lithium battery SOC rule (the rule formulated according to the state of charge and load power change in energy storage equipment) and particle swarm optimization algorithm is proposed to solve this problem. The simulation results show that the proposed strategy improves the equalization speed and accuracy of the SOC of energy storage devices, fully realizes the characteristics of different energy storage devices, and reduces the life loss of energy storage devices.

Keywords: clean energy vessel; SOC equilibrium; variable sag slope; variable filter time constant; particle swarm optimization algorithm



Citation: Ma, Z.; Chen, H.; Han, J.; Chen, Y.; Kuang, J.; Charpentier, J.-F.; Ait-Ahmed, N.; Benbouzid, M. Optimal SOC Control and Rule-Based Energy Management Strategy for Fuel-Cell-Based Hybrid Vessel including Batteries and Supercapacitors. *J. Mar. Sci. Eng.* **2023**, *11*, 398. <https://doi.org/10.3390/jmse11020398>

Academic Editors: Andrea Coraddu, Rodolfo Taccani and Federico Ustolin

Received: 10 January 2023

Revised: 6 February 2023

Accepted: 10 February 2023

Published: 10 February 2023



Copyright: © 2023 by the authors. Licensee MDPI, Basel, Switzerland. This article is an open access article distributed under the terms and conditions of the Creative Commons Attribution (CC BY) license (<https://creativecommons.org/licenses/by/4.0/>).

1. Introduction

In recent years, FCs have received much attention in the marine field because they do not produce harmful greenhouse gases [1–3]. They are particularly relevant for small or average power vessels (a few hundred kW of rated power). However, when a highly varying mission profile is considered for an FC-powered vessel, the slow response of FCs cannot provide timely power to complex and dramatically fluctuating loads. Therefore, FCs need to be equipped with fast-response energy storage devices to be able to provide the required power during transient states. It is also necessary to consider the problem caused by the variation in the SOC among energy storage devices [4,5]. It is required to prevent the energy storage devices from reaching their limits (low or high charge limits)

during operation, which leads to a shortened equipment life, early withdrawal from work, and dangerous shipload system operation. Therefore, it is necessary to propose control strategies considering the dynamic equalization of the SOC of vessel energy storage devices to quickly and accurately obtain the SOC of each energy storage device.

The reference [6] introduces virtual rated power to improve the accuracy of the load current distribution under the change in line resistance according to the battery SOC and virtual rated power. The reference [7] proposes a multi-intelligence-based two-quadrant adaptive sag control method to achieve the convergence of the power and SOC of distributed energy storage devices and maintain the stability of the bus voltage. The reference [8] proposes a decentralized control strategy based on the battery SOC to enable a series-parallel-structured battery ESS to distribute power according to the capacity, eliminate battery differences, prolong the life, and avoid over-discharge. The reference [9] proposes a hierarchical control strategy for distributed ESSs with different capacities, which can achieve an accurate current distribution and SOC equalization of energy storage devices with different capacities and adapt to changes in the line impedance.

The energy management strategy focuses on controlling multiple energy allocations in hybrid vessels. According to the energy management objectives of hybrid vessels, selecting appropriate energy management strategies can not only optimize the behavior of each power device and coordinate and control the flows among them but also reduce fuel consumption and emissions to a greater extent [10,11].

In reference [12], a fuzzy logic management strategy is proposed to control the output power of FCs and ESSs according to fuzzy logic rules to improve the economy of vessel hybrid power systems. In reference [13], an energy management strategy based on a support vector machine and frequency control was proposed to optimize the filter time constant and the capacity parameters of the composite power supply using a whale-finding algorithm to improve the performance of the vessel hybrid power system. The reference [14] proposed an operation model of a hybrid electric vessel with economic scheduling considering battery life loss, which can improve the durability of the battery, the economy, and the environmental friendliness of the ship operation. The reference [15] proposed a full cycle power fluctuation smoothing strategy applied to hybrid electric vessels to optimally schedule the diesel generator, improve the operating efficiency and stability of the vessel system, and reduce power loss.

In this paper, a hybrid FC excursion vessel, “Alsterwasser”, is used as the research subject [11]. In the studied case, the vessel is powered by a FC and associated with a battery bank and supercapacitors. The objective of this paper is to study and optimize the energy management strategy of the hybrid vessel system considering, in particular, the control strategy of the hybrid marine ESSs. The functional relationship between the dynamic compensation factor and the SOC of the energy storage devices is improved to enhance the speed and accuracy of SOC equalization, and the stability analysis of the system with this improved method is evaluated. A power allocation strategy based on a variable time constant filter of the SOC of the energy storage devices are used to improve the output power allocation of the lithium batteries and power-based supercapacitors. Taking the aging cost and energy consumption cost of the power generation equipment as optimization goals and considering the depth of discharge of the energy storage equipment, the selection of the spatial extent of the particle swarm search is improved in the particle swarm optimization (PSO) algorithm. The selection is in accordance with the determination rule based on the lithium battery SOC to achieve the goal of reasonable hydrogen consumption and reduce the life loss of the energy storage equipment.

2. Vessel Hybrid Power Systems

This paper takes the “Alsterwasser” tourism vessel as the research subject [11]. The hybrid power system of this vessel is composed of an FC system, three ESSs (two lithium battery packs and a supercapacitor pack), DC/DC converters (which allow the ESSs and FC to be connected to a common DC bus), and a shipload representing the vessel propulsion

power demand and hotel load. Figure 1 below shows the block diagram of the structure of the vessel’s hybrid power system. The power demand in a working cycle is shown in Figure 2. This power demand will be considered the typical working cycle for all the studied cases. The energy management system calculates the reference output power of the FC system and converts it into the output reference current. This reference current is used to control the FC DC/DC converter to output the reference current in constant current mode. A filter is used to determine the reference of exchanged power between the different ESSs and the DC bus. The time constants of this filter are adjusted according to the determined rules. At the same time, variable sag slope control is used to equalize the two lithium battery packs’ SOC. These methods allow the control of the DC/DC converters associated with each ESS.

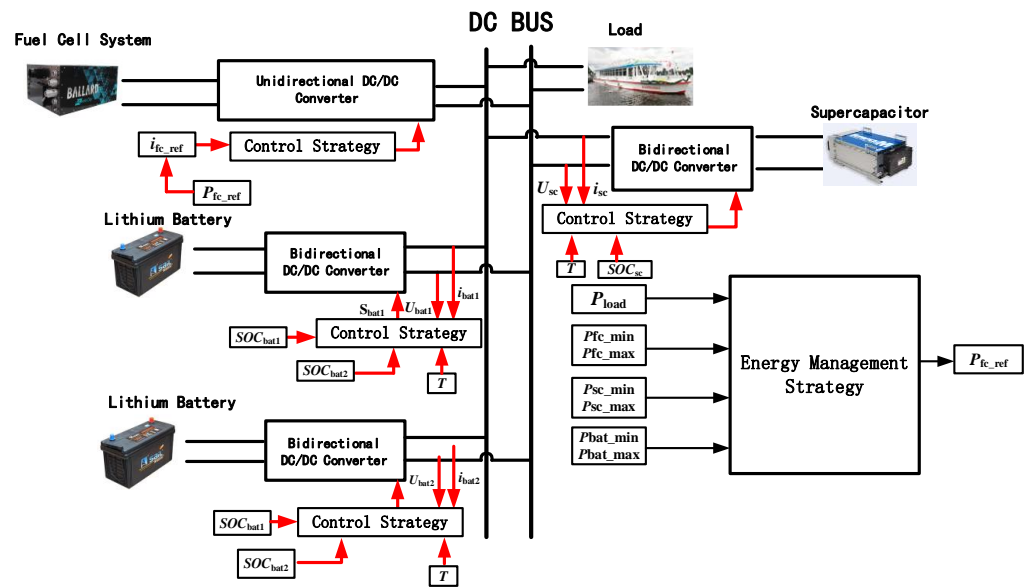


Figure 1. Block diagram of the structure of the vessel hybrid power system.

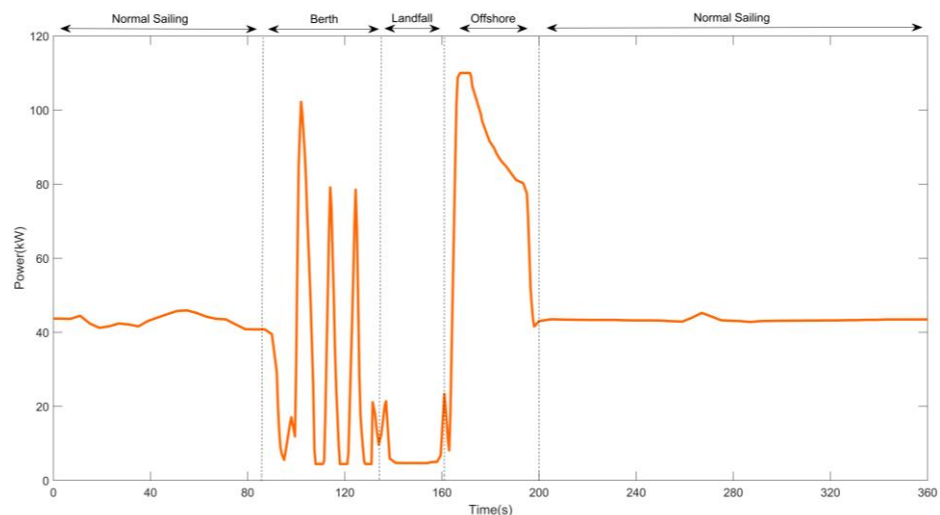


Figure 2. Power demand in a working cycle (from [11]).

3. Sag Control Strategy Based on SOC Equalization of Vessel ESS

3.1. Traditional Sag Control

Figure 3 shows the equivalent circuit of two energy storage modules connected in parallel and supplying a common load. R_{di} , R_{linei} , i_{dci} , and U_{dci} represent the virtual resistance, line resistance, output current, and output voltage of the i th DC/DC converter,

respectively. U_{dcv} , U_{dc}^* , and R_{load} represent the DC voltage on the grid side, converter output voltage reference value, and load resistance, respectively. The corresponding electrical equations of this equivalent circuit are shown in Equation (1).

$$\begin{cases} U_{dcv} = U_{dc}^* - i_{dc1}(R_{d1} + R_{line1}) \\ U_{dcv} = U_{dc}^* - i_{dc2}(R_{d2} + R_{line2}) \end{cases} \quad (1)$$

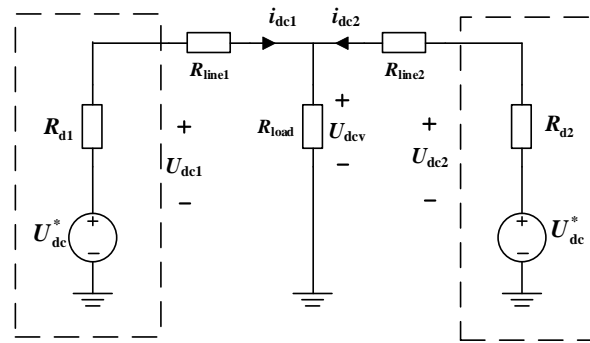


Figure 3. Equivalent circuit diagram of two energy storage modules connected in parallel.

Equation (1) arises from the output current relationship between the two DC/DC converters.

$$\frac{i_{dc1}}{i_{dc2}} = \frac{R_{d2} + R_{line2}}{R_{d1} + R_{line1}} = \frac{R_{d2}}{R_{d1}} + \frac{R_{line2} - \frac{R_{line1} \cdot R_{d2}}{R_{d1}}}{R_{d1} + R_{line1}} \quad (2)$$

The following requirements need to be met to provide a more accurate current distribution (by satisfying the following Equation (3) to satisfy the current distribution mode shown in Equation (4), the current control more explicit) between the converters connected in parallel.

$$\frac{R_{d1}}{R_{d2}} = \frac{R_{line1}}{R_{line2}} \quad (3)$$

The output current relation between the two converters is

$$\frac{i_{dc1}}{i_{dc2}} = \frac{R_{d2}}{R_{d1}} \quad (4)$$

The deviation value of the bus voltage can be expressed as

$$\Delta U_{dc} = i_{dci} \cdot R_{linei} (i = 1, 2) \quad (5)$$

The choice of sag factor is a function of the maximum allowable bus voltage deviation and the maximum allowable converter output current. ΔU_{dcmax} is the maximum allowable voltage dip of the bus, and i_{dcmax} is the output current at full load of the converter.

$$0 < R_{di} \leq \frac{\Delta U_{dcmax}}{i_{dcmax}} \quad (6)$$

From the above equation, controlling the output current of the DC/DC converter can be achieved by adjusting the virtual impedance of the converter.

According to the above theoretical analysis, the sag coefficient of each converter is fixed if the conventional sag control is used. If the sag control factor or line impedance is inconsistent, the equivalent output impedance of each converter is not equal, which leads to the inconsistent output current of the converter, which puts the SOC of the energy storage device in disequilibrium, as well as leads to excessive charging and discharging of

the energy storage devices, shortening the service life of the energy storage devices, and affecting the stability of the vessel microgrid.

Therefore, the sag factor must adaptively adjust according to the SOC of each energy storage device to control the output power of the energy storage device.

3.2. Distributed Variable Sag Slope Control

The sag slope can be changed by changing the magnitude of the virtual impedance in the sag control. By combining the dynamic compensation factor with the SOC of the energy storage devices to construct a functional relationship, the energy storage devices apply this variable sag slope control based on SOC equalization, which can make the SOC gradually converge among the energy storage devices.

In parallel ESSs, the SOC equalization method can use centralized, decentralized, and distributed control [16–19]. Among them, distributed control has higher reliability and stability and can make energy storage equipment’s SOC equalization faster and more accurate due to its high reliability and stability. Therefore, this paper investigates the distributed variable sag slope control based on SOC equalization [20]. The principle of this method is shown in Figure 4.

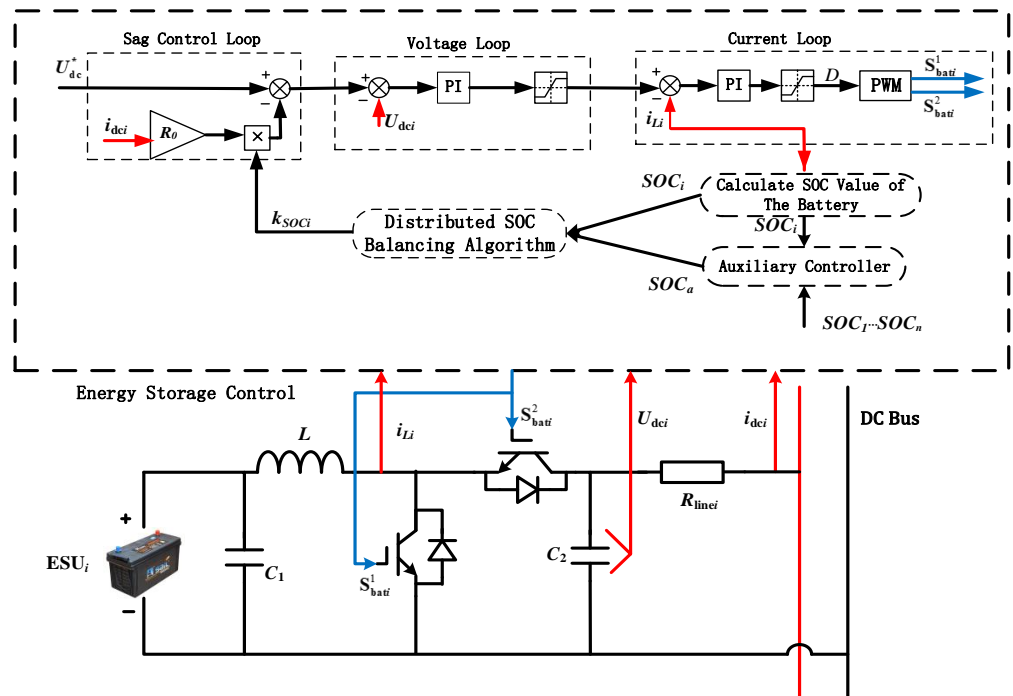


Figure 4. Distributed variable sag slope control schematic.

Estimation of SOC energy storage is conducted using the classical coulomb counting method with the following equation:

$$SOC_i(t) = SOC_i(0) - \frac{1}{C_{essi}} \int_0^t i_{essi} dt \tag{7}$$

where $SOC_i(t)$ is the SOC value of the i th unit of the distributed energy storage at time t , C_{essi} is the rated capacity of the i -th distributed energy storage unit, and i_{essi} is the output current of the i -th distributed energy storage unit.

The rate of change in the SOC can be obtained using the above equation,

$$SOC'_i(t) = -\frac{i_{essi}}{C_{essi}} \tag{8}$$

which leads to

$$SOC'_i(t) = -\frac{U_{dc}^* - U_{dci}}{C_{essi}R_{di}} \tag{9}$$

From the above equation, it can be seen that the SOC equalization of energy storage devices can be achieved by dynamically adjusting the sag factor. The distributed variable sag slope control equation is

$$U_{dci} = U_{dc}^* - R_{SOCi} \cdot i_{dci} \tag{10}$$

where R_{SOCi} is the improved sag factor with the following expression:

$$R_{SOCi} = R_0 \cdot k_{SOCi} \tag{11}$$

where R_0 represents the initial sag factor, and k_{SOCi} represents the dynamic compensation factor of the sag factor. Combining Equations (10) and (11), the output current of the i -th DC/DC converter is

$$i_{dci} = \frac{U_{dc}^* - U_{dci}}{R_0 k_{SOCi}} \tag{12}$$

The classical distributed variable sag slope control strategy based on SOC equalization has a slow rate of equalization, as shown in [20]. The objective of this paper is to propose an improved distributed variable sag slope control strategy for SOC equalization by adding factors to the functional relationship between the dynamic compensation factor k_{SOCi} and the SOC of the energy storage device in order to better regulate the sag coefficient change and to improve the speed and accuracy of SOC equalization. The improved expression for the dynamic offset factor k_{SOCi} is

$$k_{SOCi} = \begin{cases} \frac{SOC_i}{SOC_a} e^{\frac{\zeta}{\alpha|SOC_i^n - SOC_a^n| + \beta} (SOC_i^n - SOC_a^n)}, & i_{dci} < 0 \\ \frac{SOC_a}{SOC_i} e^{\frac{-\zeta}{\alpha|SOC_i^n - SOC_a^n| + \beta} (SOC_i^n - SOC_a^n)}, & i_{dci} > 0 \end{cases} \tag{13}$$

Equation (13) is defined using several tuning factors: ζ is the initial velocity factor in the SOC equalization, which affects the initial velocity of SOC equilibrium; α is the velocity factor, which mainly affects the equilibrium velocity of the SOC; β is the accuracy factor, which is mainly used to control the final accuracy of the SOC; n is the convergence factor, which affects the convergence velocity and convergence effect of the SOC.

To simplify the derivation process, it is assumed that

$$F_i = \frac{\zeta}{\alpha|SOC_i^n - SOC_a^n| + \beta} \tag{14}$$

If the process of discharging two parallel connected energy storage units is considered, substituting Equations (11)–(14) into Equation (7) leads to

$$SOC_i(t) = SOC_i(0) - \int_0^t \frac{SOC_i(t)(U_{dc}^* - U_{dci})}{C_{bati}R_0SOC_a(t)e^{F_i(SOC_a^n - SOC_i^n)}} dt \tag{15}$$

Considering $U_{dc1} = U_{dc2} = U_{dc}$, $C_{bat1} = C_{bat2} = C_{bat}$, the difference in the SOC of two distributed energy storage units is

$$\begin{aligned} \Delta SOC_{12}(t) &= SOC_1(t) - SOC_2(t) \\ &= SOC_1(0) - SOC_2(0) - \int_0^t \frac{SOC_1(t)(U_{dc}^* - U_{dc1})}{C_{bat}R_0SOC_a(t)e^{F_1(SOC_a^n - SOC_1^n)}} dt \\ &\quad + \int_0^t \frac{SOC_2(t)(U_{dc}^* - U_{dc2})}{C_{bat}R_0SOC_a(t)e^{F_2(SOC_a^n - SOC_2^n)}} dt \end{aligned} \tag{16}$$

The derivation of the above Equation (15) is

$$\begin{aligned} \Delta SOC'_{12}(t) &= \frac{SOC_2(t)(U_{dc}^* - U_{dc})}{C_{bat}R_0SOC_a(t)e^{F_2(SOC_a^n - SOC_2^n)}} - \frac{SOC_1(t)(U_{dc}^* - U_{dc})}{C_{bat}R_0SOC_a(t)e^{F_1(SOC_a^n - SOC_1^n)}} \\ &= \frac{(U_{dc}^* - U_{dc})}{C_{bat}R_0SOC_a(t)} \cdot \left(\frac{SOC_2(t)}{e^{F_2(SOC_a^n - SOC_2^n)}} - \frac{SOC_1(t)}{e^{F_1(SOC_a^n - SOC_1^n)}} \right) \end{aligned} \quad (17)$$

According to the above Equations (16) and (17), when $SOC_1(0) < SOC_2(0)$, then $\Delta SOC_{12}(t) < 0$, $\Delta SOC'_{12}(t) > 0$. Similarly, when $SOC_1(0) > SOC_2(0)$, then $\Delta SOC_{12}(t) > 0$, $\Delta SOC'_{12}(t) < 0$. This means that $\Delta SOC_{12}(t)$ will gradually decrease to zero with time t (stable process). The difference in the SOC between the two parallel connected energy storage units gradually decreases, as shown in Figure 5.

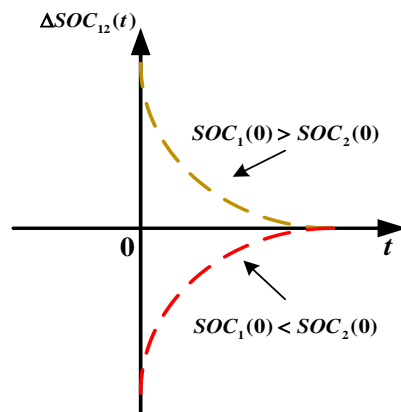


Figure 5. $\Delta SOC_{12}(t)$ convergence curve.

Under the assumption that R_0 is a given value, the plot of ΔSOC versus R_{SOCi} is shown in Figure 6 below for the process of discharging a distributed energy storage device; when the n, ζ, α , or β factor is varied, the other three factors are fixed.

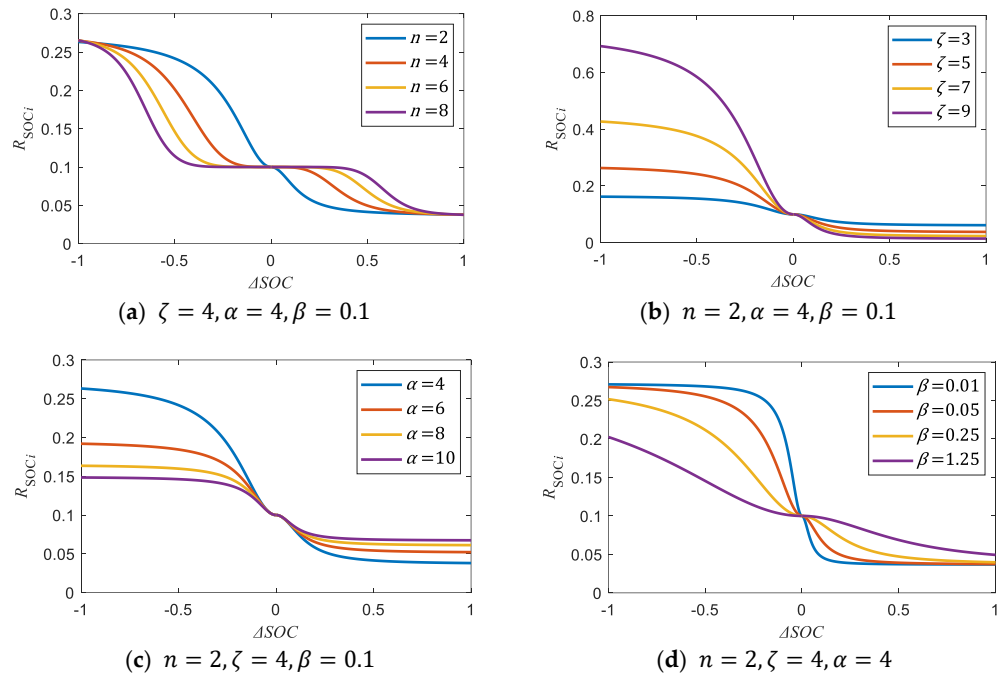


Figure 6. ΔSOC as a function of R_{SOCi} for several factor set values.

From Figure 6, we can see that when the energy storage device is operating in discharge mode, energy storage devices with less power reduce the discharge current by increasing ζ and decreasing n, α , or β so that the sag factor is larger, whereas the energy storage device with more power increases the discharge current by increasing the value of ζ and decreasing n, α , or β so that the sag factor is smaller.

According to Equation (13), when $|\Delta SOC_{12}^n|$ is larger, $\alpha |\Delta SOC_{12}^n| \gg \beta$, the equalization speed is mainly affected by α, ζ , and n . When $|\Delta SOC_{12}^n|$ is small, $\alpha |\Delta SOC_{12}^n| \approx 0$, the equilibrium velocity is mainly influenced by β and ζ . The $\frac{SOC_a}{SOC_i}$ and $\frac{SOC_i}{SOC_a}$ in Equation (13) can also play the role of regulating the sag coefficient to different degrees.

3.3. Stability Analysis

The stability analysis of a system applying distributed variable sag slope control with improved SOC equalization is presented as an example of a vessel DC microgrid [21]. The equivalent model of the i -th energy storage device for stability analysis is shown in Figure 7. $G_{\omega_c}(s) = \frac{\omega_c}{s + \omega_c}$ is the transfer function of the first-order low-pass filter, which is used to simulate the filter link of the actual sampling module. $G_d(s) = \frac{1}{s + 1}$ is the transfer function of the delay, which is used to simulate the control delay of the actual system. $G_c(s) = \frac{1}{(\tau s + 1)}$ is the closed-loop DC voltage transfer function; in general, $G_c(s)$ is approximately 1.

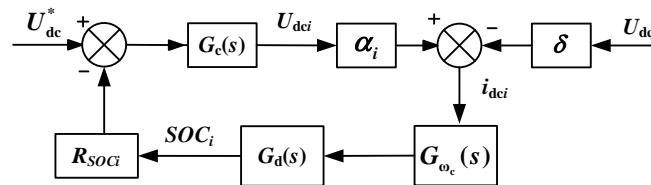


Figure 7. Equivalent model for stability analysis.

From Figure 7 above, the following equation can be obtained:

$$\begin{cases} U_{dci}(s) = U_{dc}^* - R_{SOCi} \frac{1}{s+1} \frac{\omega_c}{s+\omega_c} (\alpha_i U_{dci} - \delta U_{dcj}) \\ U_{dcj}(s) = U_{dc}^* - R_{SOCj} \frac{1}{s+1} \frac{\omega_c}{s+\omega_c} (\alpha_j U_{dcj} - \delta U_{dci}) \end{cases} \quad (18)$$

where

$$\begin{cases} \alpha_i = \frac{R_{linej} + R_{load}}{R_{linei} R_{linej} + R_{linei} R_{load} + R_{linej} R_{load}} \\ \alpha_j = \frac{R_{linei} + R_{load}}{R_{linei} R_{linej} + R_{linei} R_{load} + R_{linej} R_{load}} \\ \delta = \frac{R_{load}}{R_{linei} R_{linej} + R_{linei} R_{load} + R_{linej} R_{load}} \end{cases} \quad (19)$$

In the above set of equations, R_{linej} , R_{linei} , and R_{load} are the j -th line impedance, the i -th line impedance, and the load impedance, respectively. Combining Equations (10), (18), and (19), the system characteristic equation can be derived:

$$as^4 + bs^3 + cs^2 + ds + e = 0 \quad (20)$$

where

$$\begin{cases} a = 1 \\ b = 2 + 2\omega_c \\ c = 1 + 4\omega_c + \omega_c^2 - (\alpha_i + \alpha_j) R_{SOC} \\ d = 2\omega_c + 2\omega_c^2 - (\alpha_i + \alpha_j) (1 + \omega_c) \omega_c R_{SOC} \\ e = \omega_c^2 - (\alpha_i + \alpha_j) \omega_c^2 R_{SOC} + (\alpha_i \alpha_j - \delta^2) (\omega_c R_{SOC})^2 \end{cases} \quad (21)$$

The characteristic equation of the control system needs to satisfy the Routh stability criterion: $(a, b, c, d, e) > (0, 0, 0, 0, 0)$. The value of the sag coefficient is determined by the Routh stability criterion and Equation (6).

The root trajectory of the variation in the cutoff frequency ω_c and the sag coefficient R_{SOCi} is plotted according to the parameters related to the stability analysis shown in Table 1 below, as shown in Figure 8. From the graph, it can be seen that the dominant pole and conjugate pole are on the negative half-axis of the real axis as the sag coefficient and cutoff frequency increase, and thus the stability of the system can be guaranteed.

Table 1. Parameters related to stability analysis.

Parameters	Value
R_{load}	100 Ω
R_{linei}	2 Ω
R_{linej}	1 Ω
R_{SOCi}	0.1 ~ 0.8 Ω
ω_c	20~100 rad/s

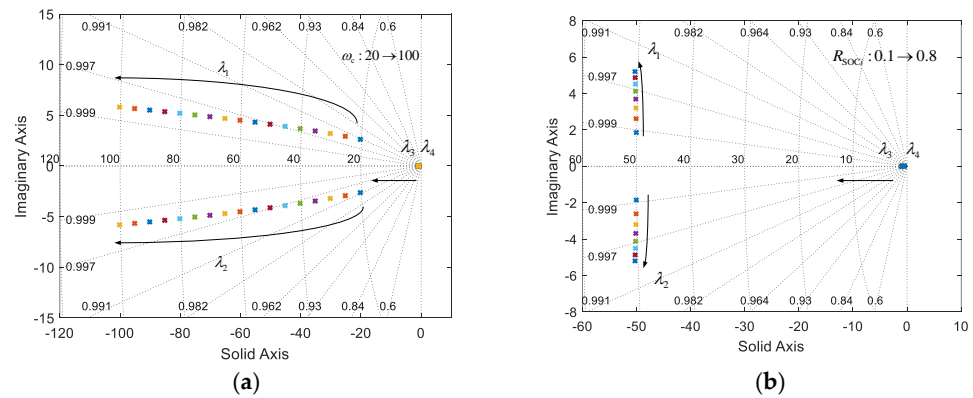


Figure 8. Root trajectory diagram: (a) cutoff frequency change; (b) change in sag factor.

4. Energy Management Strategies for Marine Hybrid Power Systems

The energy management strategy for the hybrid vessel power system in this paper is proposed based on the following three strategies: SOC supercapacitor operating mode switching strategy, hybrid energy storage unit power allocation strategy, and hybrid FC vessel energy management strategy. A working mode switching strategy is applied to control the depth of charging and discharging of the supercapacitor; a hybrid power allocation strategy for energy storage units is applied to improve the reasonableness of the power allocation at the output of the energy-based lithium battery and the power-based supercapacitors; the energy management strategy of the hybrid FC vessel is applied to achieve the goal of reasonable hydrogen consumption and reduced life loss of the energy storage equipment.

4.1. Operating Mode Switching Strategy Based on Supercapacitor SOC

In this paper, rules are proposed to prevent supercapacitors from charging and discharging excessively, resulting in a shortened service life and performance. These rules are based on switching between constant voltage and constant current charging and discharging modes depending on the SOC value of the supercapacitors. These switching rules are controlled by a hysteresis loop, which can prevent the supercapacitor from immediate alternative switching when the SOC reaches the test value. Using hysteresis allows for reducing the number of switches from one strategy to another. Figure 9 shows the operating mode switching principle of the supercapacitor, and Figure 10 shows the hysteresis loop switching principle.

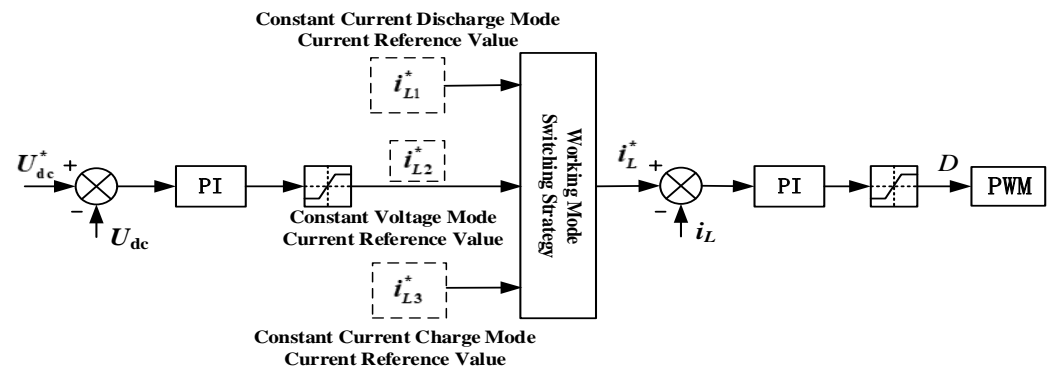


Figure 9. Principle diagram of supercapacitor operating mode switching.

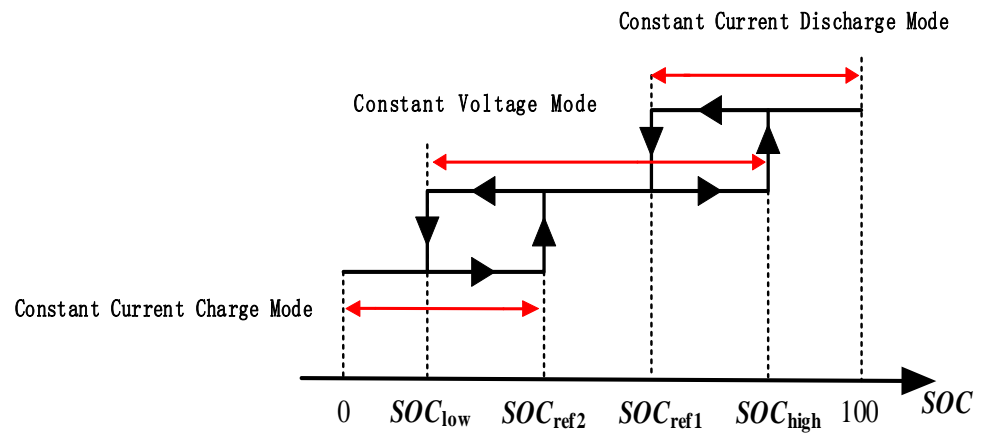


Figure 10. Supercapacitor operating mode hysteresis loop switching diagram.

4.2. Hybrid Energy Storage Unit Power Allocation Strategy

It is a critical issue to allocate the output power of FCs, lithium batteries, and supercapacitors and maintain the balance of instantaneous power between the system components during a sudden change in load power. Considering the simplicity and efficiency of use, first-order high- and low-pass filters are applied between the voltage and current loops in this paper, as shown in Figure 11 below.

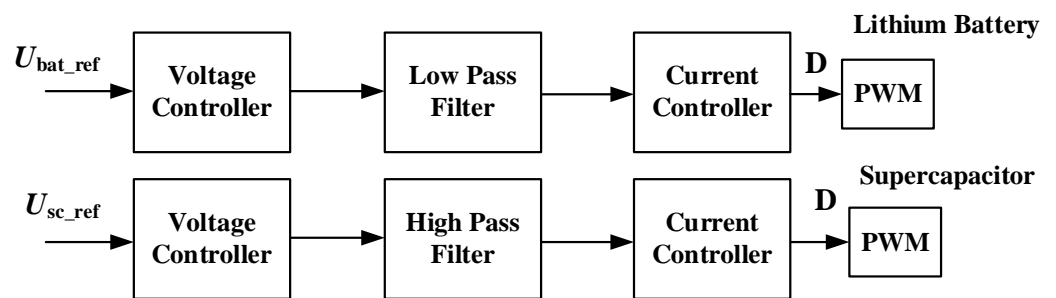


Figure 11. Control block diagram with filter added between the double closed loop.

In Figure 11, U_{bat_ref} and U_{sc_ref} indicate the voltage reference values of the lithium battery and the supercapacitor, respectively, while D indicates the duty ratio.

Since the vessel hybrid system model built in this paper is a discrete simulation model, the first-order filter transfer function has to be converted into a discrete form. The discrete transfer functions of the low-pass and high-pass filters are as follows [22]:

$$Y(n) = \frac{1}{1 + \frac{T}{\Delta T}} X(n) + \frac{\frac{T}{\Delta T}}{1 + \frac{T}{\Delta T}} Y(n - 1) \tag{22}$$

$$Y(n) = \frac{T}{T + \Delta T} \cdot (X(n) - X(n - 1) + Y(n - 1)) \tag{23}$$

where $X(n)$ denotes the n -th sampling value, $Y(n)$ denotes the n -th filter value, ΔT is the sampling period, and T is the time constant. From the above equation, it can be seen that the system can control the power of the energy storage device by adjusting the filter time constant T .

In order to improve the reasonableness of allocating lithium battery and supercapacitor power when the vessel’s charging power fluctuates, and to ensure that the vessel is able to operate safely and stably for an extended period of time, in this paper, we adopt a power allocation strategy with variable filter time constants. With this strategy, the vessel can adjust the filter time constant based on the SOC and phase of operation of the lithium battery and supercapacitor, and the rule of determination is given in Table 2 below.

Table 2. Table of rules for variable filter time constants.

	$SOC_{ess} < SOC_{min}$	$SOC_{min} \leq SOC_{ess} \leq SOC_{max}$	$SOC_{max} \leq SOC_{ess}$
Normal Navigation Phase	$T_{bat} = T_{b_max1}$ $T_{sc} = T_{s_min1}$	$T_{bat} = T_{b_median1}$ $T_{sc} = T_{s_median1}$	$T_{bat} = T_{b_min1}$ $T_{sc} = T_{s_max1}$
Port Call, Shore, and Offshore Phase	$T_{bat} = T_{b_max2}$ $T_{sc} = T_{s_min2}$	$T_{bat} = T_{b_median2}$ $T_{sc} = T_{s_median2}$	$T_{bat} = T_{b_min2}$ $T_{sc} = T_{s_max2}$

In the table, $T_{b_min1} < T_{b_min2} < T_{b_median1} < T_{b_median2} < T_{b_max1} < T_{b_max2}$, $T_{s_min1} < T_{s_min2} < T_{s_median1} < T_{s_median2} < T_{s_max1} < T_{s_max2}$, SOC_{ess} for the energy storage device’s own SOC.

Considering the load profile in Figure 2, in the vessel mooring, alongside, and offshore stages where the load power sharply fluctuates, by convolving the time constants in both the high- and low-pass filters, the supercapacitor will improve the speed of response, increase the output power, and take on more high-frequency power. The lithium battery will reduce the speed of response, and the high-frequency charging power it takes on will be reduced. This method can achieve the effect of “Cutting the peak and filling the valley”.

This strategy makes full use of the characteristics of energy-type lithium batteries outputting a higher amount of power for a long time to meet the energy demand of the hybrid vessel. It also gives full play to the characteristics of power-type supercapacitors outputting high-frequency power for a short time to improve the power quality of the hybrid vessel system. Further, it also prevents the problem of increasing the discharge power of low-capacity energy storage devices, leading to their over-discharge, shortening their life, and affecting their performance.

4.3. Hybrid FC Vessel Energy Management Strategy

In this paper, two energy management objectives are considered, namely, equipment lifetime and energy cost [23,24]. These two objectives are combined into the form of a global objective of minimizing the power supply cost. The frequent fluctuation in the power source power is one of the factors that reduces the service life, so the fluctuation value of

power is taken as an objective function that affects the service life. The conventional vessel energy management strategy constructed in this paper has the following objective function:

$$J_{\min} = \begin{bmatrix} C_{fc, \text{sum}} \\ C_{bat, \text{sum}} \\ C_{sc, \text{sum}} \end{bmatrix} \tag{24}$$

where $C_{fc, \text{sum}}$, $C_{bat, \text{sum}}$, $C_{sc, \text{sum}}$ are the total working costs for the FC, lithium battery, and supercapacitor, respectively.

$$C_{x, \text{sum}} = C_{x, \text{life}} + C_{x, \text{eco}} \tag{25}$$

$$C_{x, \text{life}} = m_x \sum_{t=1}^T (P_x(t) - P_x(t-1))^2 \tag{26}$$

$$C_{fc, \text{eco}} = \sum_{t=1}^T C_{H_2} \cdot K^{m-v} \cdot K^{E-m} \cdot (aP_{fc}^2(t) + bP_{fc}(t) + c) \tag{27}$$

$$C_{bat, \text{eco}} = \sum_{t=1}^T C_{bat, \text{ope}} \cdot P_{bat}(t) \tag{28}$$

$$C_{sc, \text{eco}} = \sum_{t=1}^T C_{sc, \text{ope}} \cdot P_{sc}(t) \tag{29}$$

where $C_{x, \text{life}}$ is the aging cost of the power generation equipment, m_x is the aging cost coefficient of the power generation equipment, $C_{x, \text{eco}}$ is the energy consumption cost of the power generation equipment, $P_x(t)$ is the output power of the power generation equipment at moment t , C_{H_2} is the price of hydrogen, K^{m-v} is the conversion factor of mass to volume, K^{E-m} is the conversion of energy to mass coefficient, a , b and c are FC output power coefficients, $C_{bat, \text{ope}}$ is the lithium battery operating cost, and $C_{sc, \text{ope}}$ is the supercapacitor operating cost.

The constraints are shown in the following equation:

$$\begin{cases} P_{fc} + P_{bat} + P_{sc} = P_{load} \\ P_{fc, \min} < P_{fc} < P_{fc, \max} \\ P_{bat, \min} < P_{bat} < P_{bat, \max} \\ P_{sc, \min} < P_{sc} < P_{sc, \max} \end{cases} \tag{30}$$

The first constraint is the constraint of the vessel power balance to ensure the stable operation of the vessel. The other constraints are related to the output power range of FCs, lithium batteries, and supercapacitors.

The evaluation function formula is shown below:

$$Z_{\min} = C_{eco} + A \cdot C_{fc, \text{life}} + B \cdot C_{bat, \text{life}} + C \cdot C_{sc, \text{life}} + D \cdot P_{bal} \tag{31}$$

$$C_{eco} = C_{fc, \text{eco}} + C_{bat, \text{eco}} + C_{sc, \text{eco}} \tag{32}$$

$$P_{bal} = (P_{load} - P_{fc} - P_{bat} - P_{sc})^2 \tag{33}$$

where C_{eco} is the total energy cost; A , B , and C are the penalty coefficients for the FC, lithium battery, and supercapacitor aging costs, respectively; D is the penalty coefficient for the vessel power balance; P_{bal} is the vessel power balance function equation. Thus, the larger the value of each power supply aging cost and power balance functional equation, the larger the value of each penalty coefficient.

The conventional vessel energy management strategy built in this paper considers only the power generation equipment's energy cost and power output fluctuation. The problem of deep-discharging energy storage equipment also needs to be taken into account.

A deep discharge depth accelerates the life shortening of energy storage equipment and affects its performance [25,26]. The battery’s depth of discharge is typically between 0.2 and 0.8 in real engineering. As an example, the number of possible cycles in the lifetime versus the discharge depth is presented in Table 3 for a typical lithium battery pack [26].

Table 3. Relationship between the depth of discharge of a lithium battery and its cycle life.

Discharge Depth	Cycle Life/Time
0.2	50,000
0.4	14,000
0.6	8000
0.8	6000
1	4000

The energy storage device life daily loss function equation is expressed by the ratio of the number of times the energy storage device is charged and discharged in a day to its entire cycle life [25].

$$f = \frac{N}{N_{sum}} \tag{34}$$

where N_{sum} is the total cycle life of the energy storage device, and N is the number of times the energy storage device is charged and discharged within a day, which is expressed by the total output power of the energy storage device and its rated capacity within a day.

$$N = \frac{\int P_{ess} dt}{Q_{ess}} \tag{35}$$

where P_{ess} is the output power of the energy storage device, and Q_{ess} is the rated capacity of the energy storage device.

The low capacitance of the supercapacitor makes it easy to change its SOC value compared to a lithium battery. This paper improves the vessel energy management strategy by combining lithium battery charge-state-based determination rules with the PSO algorithm. Table 4 shows the rules for this improved strategy. The upper and lower limits of the output power of each generation device will be changed according to the SOC value of the lithium battery using a hysteresis loop, as shown in Figure 12. Figure 13 shows the flowchart for the method combining the lithium battery SOC-based determination rules with the PSO algorithm.

Table 4. Improvement strategy table.

	FC Output Power	Lithium Battery Output Power	Ultracapacitor Output Power
State = 1	$[P_{fcmin1}, P_{fcmax1}]$	$[P_{batmin1}, P_{batmax1}]$	$[P_{scmin1}, P_{scmax1}]$
State = 2	$[P_{fcmin2}, P_{fcmax2}]$	$[P_{batmin2}, P_{batmax2}]$	$[P_{scmin2}, P_{scmax2}]$

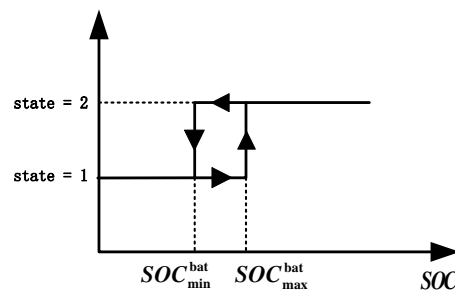


Figure 12. Upper and lower output power switching diagram for each power generation device.

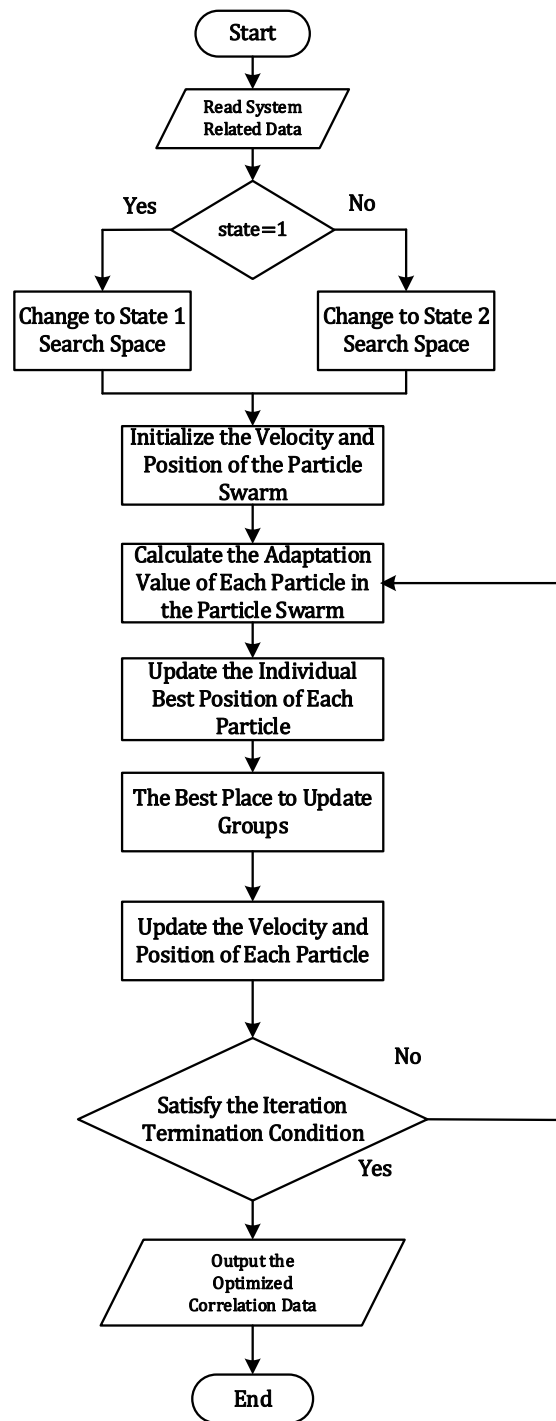


Figure 13. Flowchart of the global rules of PSO.

In the optimization of the objective function using the PSO algorithm, the power exchanged with the DC grid for FCs, lithium batteries, and supercapacitors is used as three particles with different ranges, i.e., the upper and lower limits of the output power of the three power sources are different. The output power’s higher and lower bounds of the three power supplies are adjusted based on the SOC value of the lithium battery for charging/discharging the energy storage device.

The improved strategy allows the vessel to operate steadily at any stage. At the same time, according to the SOC value of lithium batteries and the load power of vessels, the optimal power value of FCs is calculated reasonably to prevent energy storage equipment

from deepening the discharge depth, increasing loss, and over-discharging. The strategy also provides sufficient power for the vessel’s energy storage equipment to discharge in time during the load power surge phase and ensures the stability of the vessel bus voltage.

5. Analysis of Simulation Results

5.1. Analysis of Simulation Results of SOC Equalization Strategy for ESS

A simplified simulation model of the container system was constructed on the basis of Figure 14 using the simulation module of Simulink in Matlab/Simulink. The power side consists of an FC module and three parallel connected lithium battery modules. According to the parameters given in Table 5, the distributed variable sag slope control method based on SOC equalization and the improved SOC equalization method are used for the energy ESS to compare and verify the effectiveness of these two methods in equalizing the SOC under both the charging and discharging operation modes of the load [20], as well as the effectiveness of the load system.

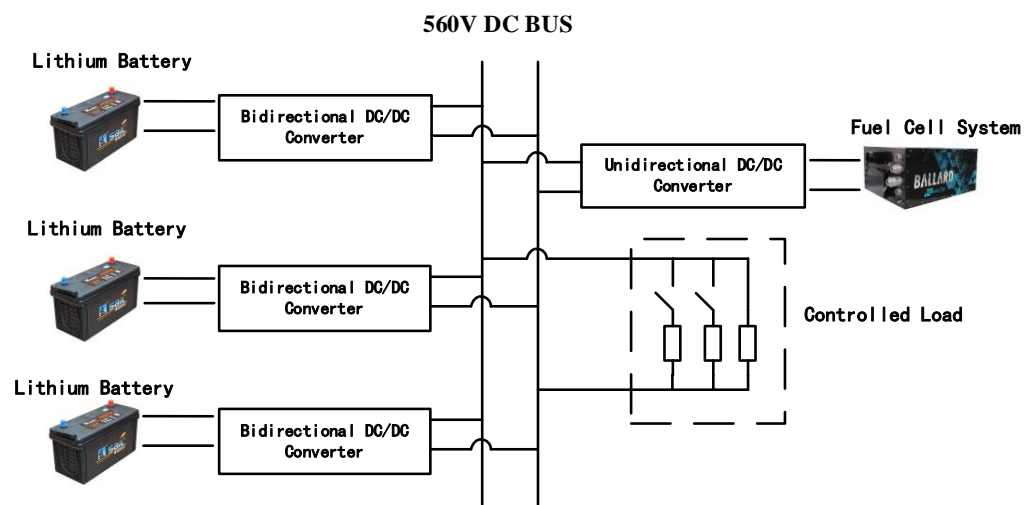


Figure 14. Simplified simulation model of the vessel system.

Table 5. Table of simulation parameters for applying sag control.

Parameter Name	Take Value	Parameter Name	Take Value
Lithium Battery Voltage	240 V	Initial Sag Factor	0.01 Ω
DC Bus Voltage	560 V	Rated Capacity of Energy Storage Module	5 Ah
Input-Side Capacity	200 μF	Output-Side Capacity	4 mF
Inductance	5 mH	Switching Frequency	10 kHz

In order to quickly observe the equalization effect of the adopted algorithm, the nominal capacity of each lithium battery module is set to 5 Ah. In the simulations presented in this paper, the effects of the line impedance, sampling filtering, and communication delay are ignored. As a means of analyzing the dynamic performance of the ESS under power fluctuations when equalizing the SOC with distributed variable sag slope control, the data for the load and FC power variations in this paper are set according to [9].

Figures 15 and 16 below show the simulated waveforms of the ESS discharging and charging for variations in the power of the load and FCs, respectively. In Figure 15, the ESS operates in a discharge mode and adopts distributed variable sag slope control on the basis of SOC equalization. In the simulation of 200 s, the SOC values and output power of the three lithium batteries gradually converge. On the other hand, the lithium battery with an initial SOC value of 70% converges to a different value compared to the other two lithium batteries. At t = 136 s, the three lithium cells’ SOC values and output powers converge to

$t = 50$ s, and as the charging power is increased from 24.1 kW to 39.2 kW, the output power of the three lithium cells is increased to maintain the stability of the bus voltage, and the bus voltage changes abruptly to 554 V and then recovers rapidly to 560 V. At 120 s, when the power output of the FC increases from 18.8 kW to 29.4 kW, the output power of the three lithium batteries is reduced to maintain the voltage stability of the bus, and the bus voltage decreases to 559 V, then increases to 564 V, and finally recovers back to 560 V.

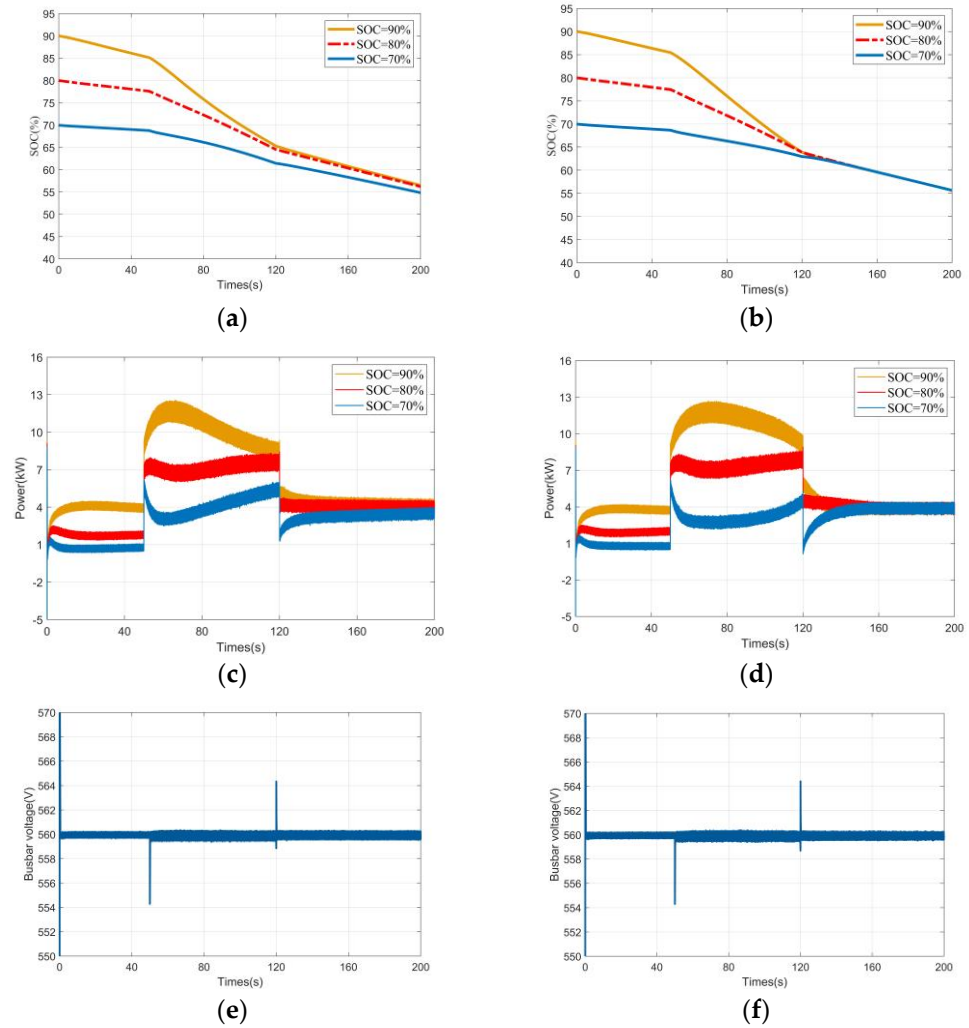


Figure 15. Simulation waveform of discharge under load and FC power variation. (a) SOC sag control, lithium battery SOC waveform; (b) improved SOC sag control, lithium battery SOC waveform; (c) SOC sag control, lithium battery power waveform; (d) improved SOC sag control, lithium battery power waveform; (e) SOC sag control, bus voltage waveform; (f) improved SOC sag control, bus voltage waveform.

In Figure 16 below, the ESS is in a charging mode with distributed variable sag slope control based on the SOC equalization for the lithium batteries. The values of the SOC and power output of the lithium battery with distributed variable sag rate control with enhanced SOC equalization converge at $t = 126$ s. At $t = 50$ s, as the charging power increases from 24.2 kW to 44.8 kW, the three lithium batteries reduce the power absorption of the FC to stabilize the voltage of the bus, and the bus voltage changes abruptly to 554 V and then recovers rapidly to 560 V. At $t = 120$ s, the FC output power increases from 60.5 kW to 72.4 kW, when the FC output power increases from 60.5 kW to 72.4 kW, the three lithium batteries increase the absorbed FC power to stabilize the bus voltage, and the bus voltage decreases to 555.4 V, then increases to 564 V, and finally recovers back to 560 V.

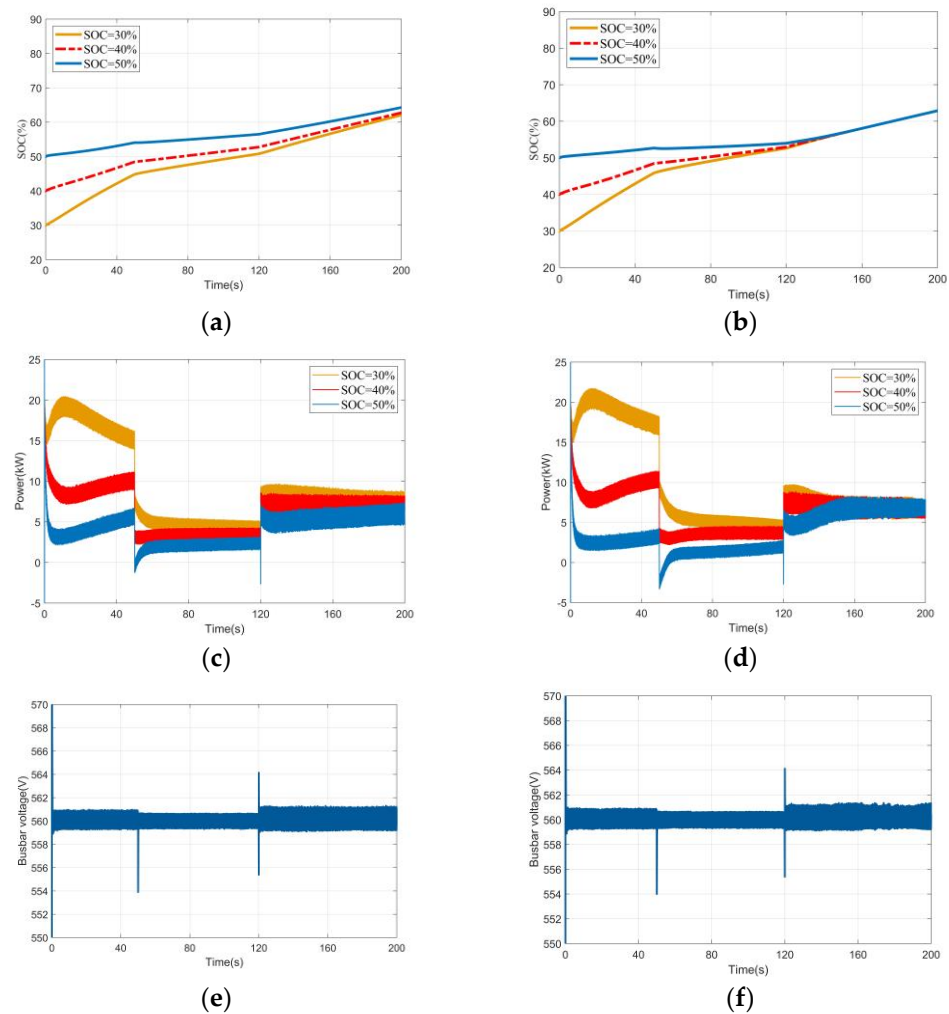


Figure 16. Simulation waveform of charging under load and FC power variation. (a) SOC sag control, lithium battery SOC waveform; (b) improved SOC sag control, lithium battery SOC waveform; (c) SOC sag control, lithium battery power waveform; (d) improved SOC sag control, lithium battery power waveform; (e) SOC sag control, bus voltage waveform; (f) improved SOC sag control, bus voltage waveform.

Consequently, both methods of variable sag slope control can control the DC bus voltage to fluctuate consistently within a reasonable range and quickly recover to the nominal value under varying load power and FC voltage. On the other hand, the distributed variable sag slope control method with improved SOC equalization can more reasonably distribute the output power and equalize the SOC values between the energy storage modules more quickly and accurately.

5.2. Analysis of Simulation Results of Power Distribution Strategy of Hybrid Energy Storage Unit

This paper uses the data in Table 6 to compare energy storage unit power allocation strategies with the application of fixed and variable filter time constants, and also to compare the energy management strategies for hybrid FC vessels with and without taking into account the depth of discharge of lithium batteries, through the analysis of relevant data from the simulation model of the hybrid power system of the vessel to verify the effect of the strategies proposed above.

Table 6. Parameter setting table of the simulation model of the vessel hybrid power system.

Category	Parameter	Numerical Value
DC Bus	Nominal Voltage	560 V
	Nominal Power	100 kW
FC	Current Loop Controller (P/I)	21.92/6232.88
	Nominal Capacity	2 × 50 Ah
Lithium Battery	Nominal Voltage	240 V
	Voltage Loop Controller (P/I)	3.5/52.5
	Current Loop Controller (P/I)	21.92/6232.88
	Initial Value of Sag Coefficient	0.3 Ω
	Nominal Capacity	63 F
Supercapacitor	Nominal Voltage	250 V
	Voltage Loop Controller (P/I)	3.5/52.5
	Current Loop Controller (P/I)	21.92/6232.88
	Constant Current Discharge Reference Current	40 A
	Constant Current Charging Reference Current	40 A
Load	Load Power	4.45~110 kW

Under the application of the distributed variable sag slope control strategy with improved SOC equalization, this section applies the power allocation strategies with fixed and variable filter time constants to compare and analyze the simulation results of the power allocation strategies of the two hybrid energy storage cells. According to the relevant dataset in the reference, the FC output power is constant at 20 kW, $SOC_{min} = 30\%$, $SOC_{max} = 80\%$, and the high- and low-pass filter time constants in the fixed filter time constant method are 5.

Comparing the output power of each power supply shown in Figures 17 and 18 above, the load power fluctuates within 90~200 s. Compared with the power stability stage, there is a large fluctuation in power, which we call high-frequency power fluctuation. The lithium battery applying the variable filter time constant method in the power fluctuation phase manages less high-frequency power than the supercapacitor applying the fixed filter time constant method, while the supercapacitor applying the variable filter time constant method manages more high-frequency power than the supercapacitor applying the fixed filter time constant method. Combined with Figures 19–21 above, during the power fluctuation phase, the system increases the high-pass and low-pass filter time constants according to the load power, the load power change rate, and the ESS’s SOC value. This is carried out so that the high-frequency power borne by the supercapacitor increases and the high-frequency power borne by the lithium battery decreases. At 279 s, the supercapacitor SOC value is lower than SOC_{min} , the system reduces the high-pass filter time constant, and the supercapacitor output power decreases accordingly, as shown in the power curve.

Thus, the simulation model can automatically adjust the filter time constant according to the different operation stages of the vessel and the SOC of the energy storage device, giving full play to the operational characteristics of the energy-type lithium battery and the power-type supercapacitor, and, at the same time, it can prevent the low-capacity energy storage device from increasing the discharge power, which leads to its over-discharge, shortens its life, and affects its performance.

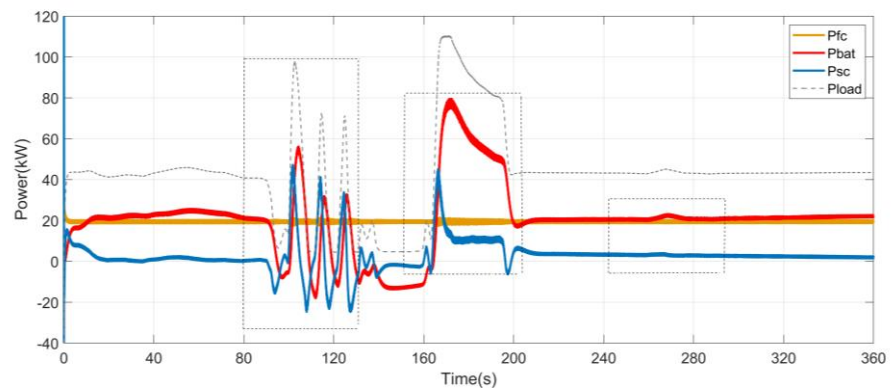


Figure 17. Power curve for a fixed filter time constant.

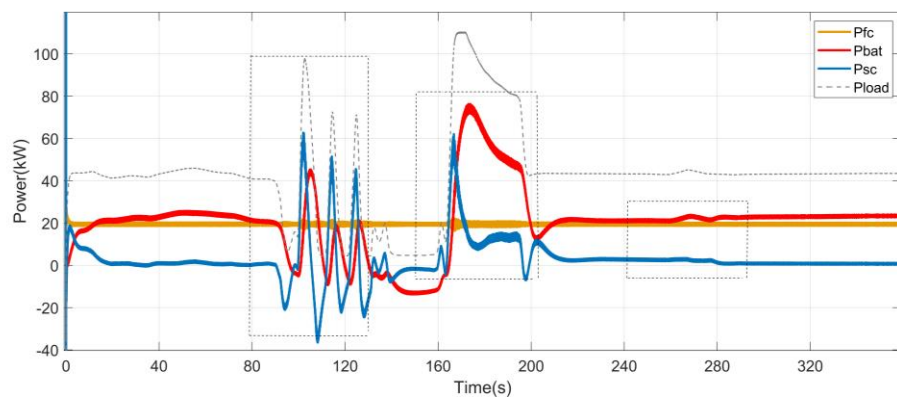


Figure 18. Power curve with variable filter time constants.

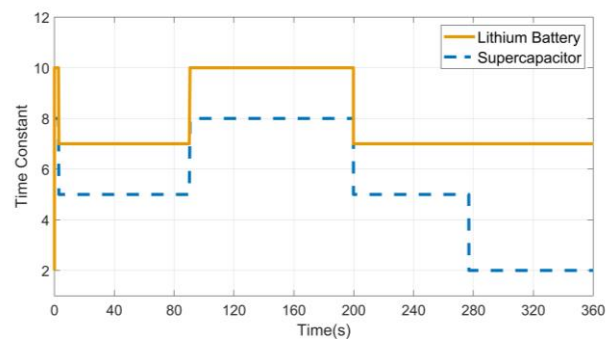


Figure 19. Variation in filter time constants for energy storage devices.

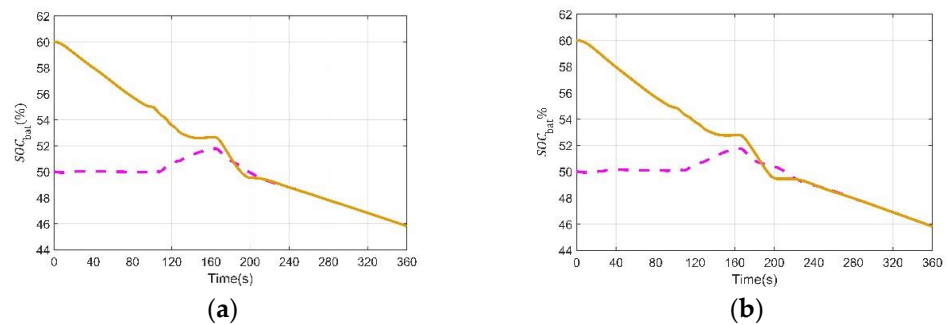


Figure 20. Comparison of the change in the SOC value of the lithium battery: (a) fixed filter time constant; (b) variable filter time constant.

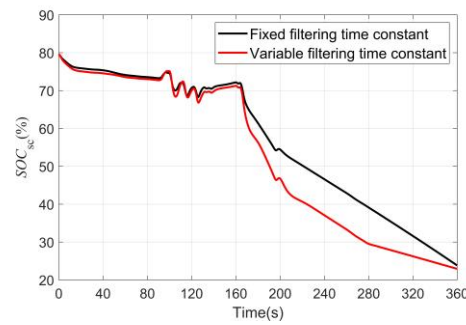


Figure 21. Comparison of the supercapacitor’s SOC value change under constant and variable filter time constants.

5.3. Analysis of Simulation Results of Energy Management Strategy for Hybrid FC Vessels

In this paper, the energy management strategy of hybrid FC vessels is simulated using the dataset in [11,13,24]. The two initial lithium battery SOC values are set to 25% and 35%, $SOC_{max}^{bat} = 30\%$, $SOC_{min}^{bat} = 20\%$. $SOC_{high} = 90\%$, $SOC_{ref1} = 80\%$, $SOC_{ref2} = 45\%$, and $SOC_{low} = 20\%$ are set to switch the supercapacitor working mode accordingly. This paper considers the rate of change in the FC output power and the power range for its efficient operation. The FC’s efficient operation should keep its output power within 10% to 90% of its maximum output power. In the PSO algorithm, the number of populations is 150, the number of iterations is 300, ω_{max} is 0.9, ω_{min} is 0.4, c_1 is 1.2, and c_2 is 0.8. According to the reference [27], the price of hydrogen is about 0.15 USD/kWh, the cost of lithium battery operation is 0.045 USD/kWh, and the cost of supercapacitor operation is 0.035 USD/kWh. Therefore, although FC operation can reduce the emission of pollutants, it requires reasonable hydrogen consumption due to its high price. According to the evaluation function of Equation (31), the PSO algorithm is applied to solve the optimal value of the objective function described above, and the FC output power with the optimal value of the objective function in the two strategies is used as the reference power and is converted into the FC reference current. It is shown in Figure 22 below.

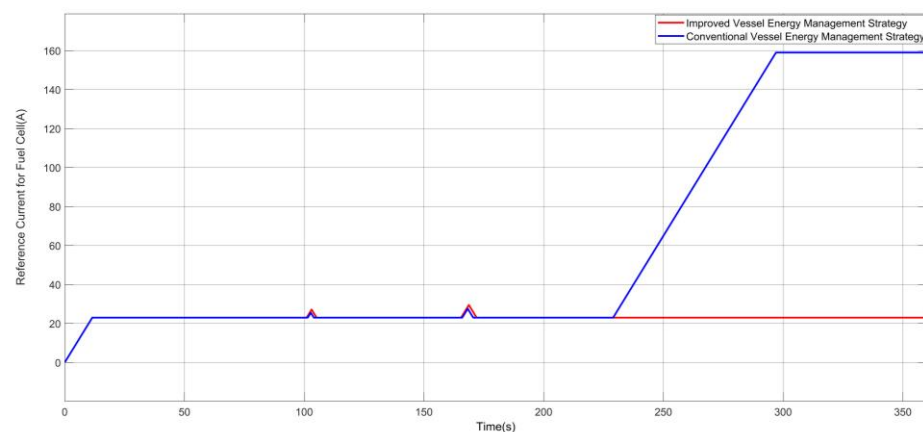


Figure 22. FC reference current curve.

In both strategies, the aging cost and energy cost are the optimization objectives, and the improved vessel energy management strategy further considers the depth of discharge of lithium batteries, unlike the conventional strategy. In order to prevent the lithium battery discharge depth from exceeding 80%, the FC system, under the improved strategy, increases the output power by increasing the hydrogen consumption to control the lithium battery discharge depth and reduce its life loss. In Figure 22, the FC output current slowly increases from 23 A to 159 A under the improved strategy. Analyzing Figures 23–25, the SOC values of both lithium batteries in both strategies converge at the simulation time of 188 s and remain the same in the subsequent time. The system applies the improved vessel

energy management strategy, and the SOC value of the lithium battery drops to SOC_{min} at 280 s. To prevent the lithium battery from discharging beyond the specified depth of discharge, the particle swarm search space in the PSO algorithm changes to the size of state 1, and due to the slow response of the FC, the FC output power needs to increase in advance. According to the evaluation function solution, the lithium battery SOC value is below 20% when the optimal value of the FC output power is 55 kW, which starts to grow slowly at 229 s. The FC with increased output power not only bears the load power in the normal sailing stage but also charges the energy storage equipment to provide sufficient high-frequency power in time for the vessel in the power fluctuation stage without seriously affecting its service life. Moreover, under the conventional vessel energy management strategy, after 260 s, the lithium battery with a SOC value of 20% continues to discharge, which can reduce hydrogen consumption in the FC system but deepen the discharge depth of the lithium battery, affecting its own service life.

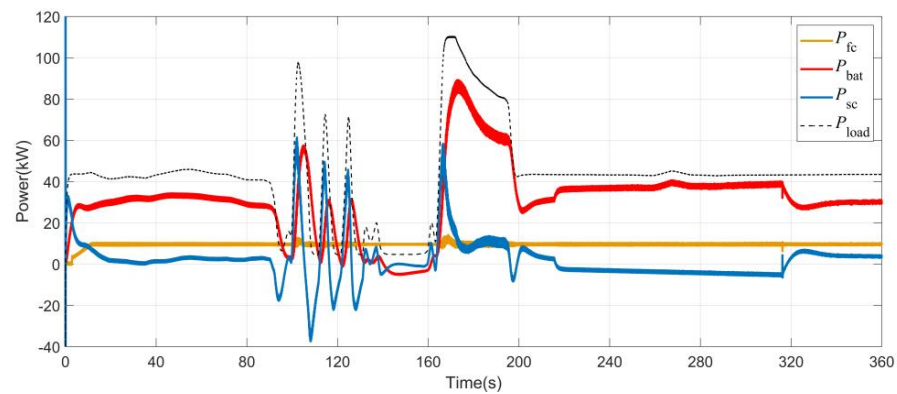


Figure 23. Power curve under the conventional vessel energy management strategy.

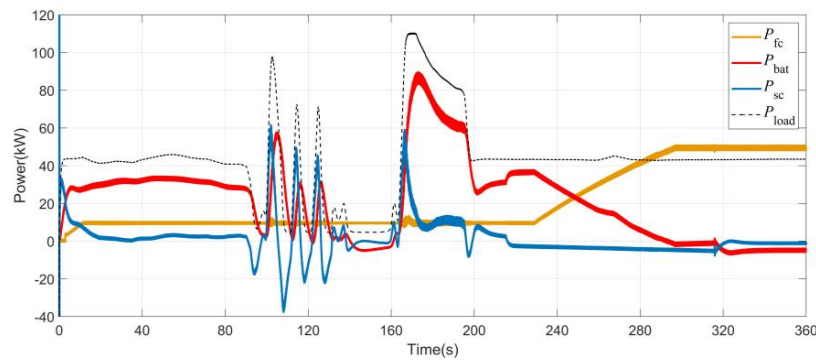


Figure 24. Power curve plot with the improved vessel energy management strategy.

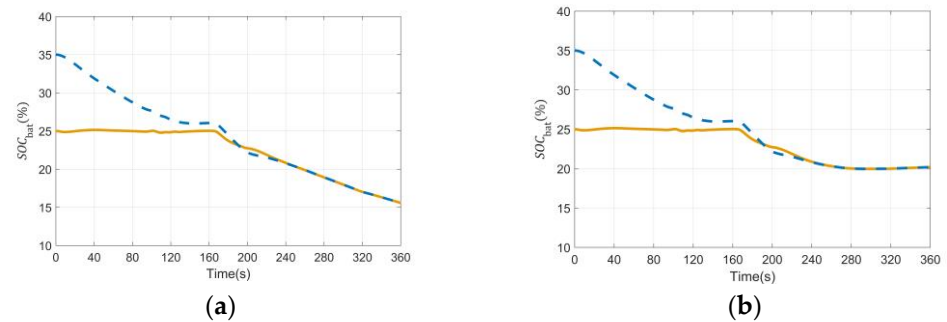


Figure 25. Variation in the SOC value of two lithium batteries under different strategies: (a) conventional vessel energy management strategy; (b) improved vessel energy management strategy.

From Figures 26 and 27, it can be seen that the supercapacitor first works in constant voltage mode, and at the simulation time of 216 s, the supercapacitor SOC value drops to SOC_{low} . The supercapacitor switches from constant voltage to constant current charging mode, and the lithium battery increases the output power to charge the supercapacitor in the conventional vessel energy management strategy. In contrast, the lithium battery first increases. In the improved vessel energy management strategy, the lithium battery output power first increases to charge the supercapacitor. At 229 s, the FC starts to increase the power gradually. The lithium battery power gradually decreases. At 285 s, the FC assumes the shipload power solely and charges the lithium batteries and supercapacitors. At 316 s, the SOC value rises to SOC_{ref2} , the supercapacitor switches back to constant voltage mode from constant current charging mode, the lithium battery output power decreases, and the supercapacitor output power increases under the conventional strategy. In contrast, the supercapacitor absorbs less power, and the lithium battery absorbs more power under the improved strategy.

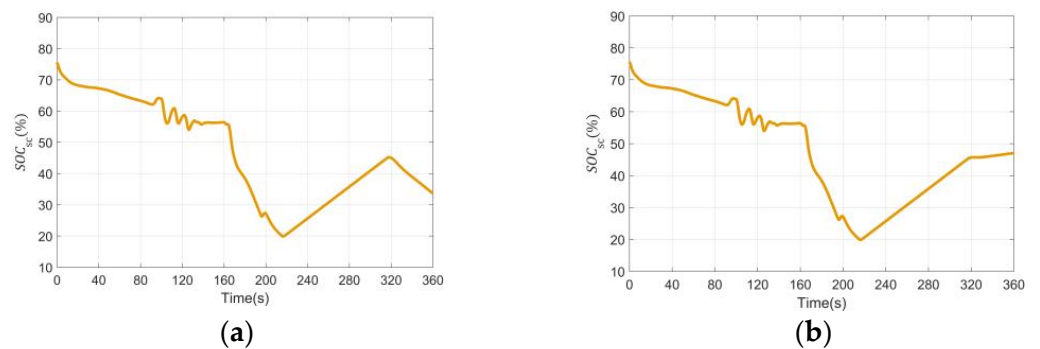


Figure 26. Variation in the SOC value of the supercapacitor with different strategies: (a) conventional vessel energy management strategy; (b) improved vessel energy management strategy.

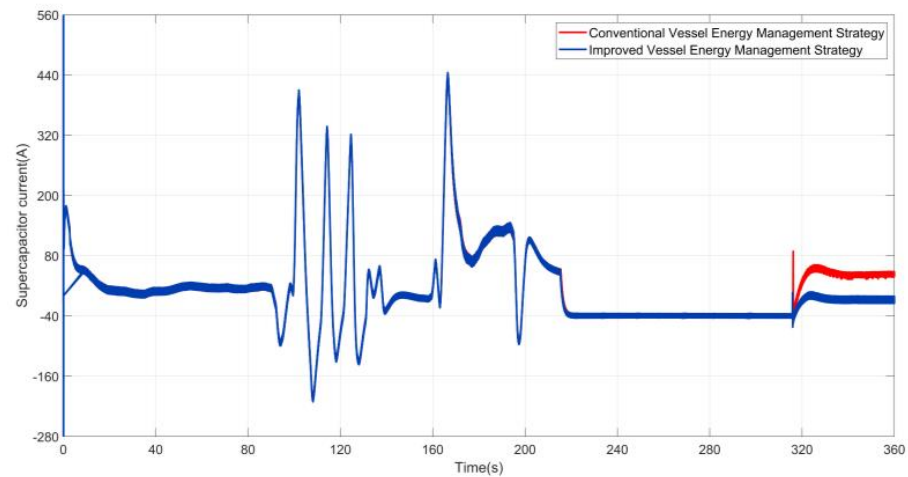


Figure 27. Variation in the supercapacitor output current under different strategies.

Generally, the bus voltage fluctuation range is $\pm 5\%$ of the rated voltage, and the maximum does not exceed $\pm 10\%$. From the bus voltage fluctuation in Figure 28, it can be seen that the bus voltage fluctuation reaches up to 579 V in the conventional strategy and up to 570 V in the improved strategy, and the bus voltage pulsation is within a reasonable range.

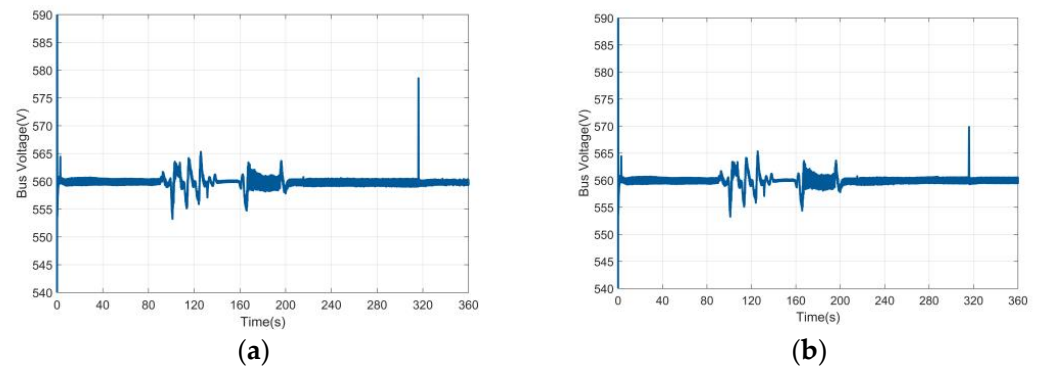


Figure 28. Bus voltage fluctuation graph for different strategies: (a) conventional vessel energy management strategy; (b) improved vessel energy management strategy.

The “Alsterwasser” excursion vessel takes half an hour to travel from Finkenwerder to Landungsbrücken with four stops in between, and the “Alsterwasser” excursion vessel works 8 h a day [24]. The hybrid FC vessel applies conventional and improved energy management strategies. The hydrogen consumption and lithium battery life loss in one day under both strategies are calculated according to the equation $\dot{m}_{fc} = \frac{Ni_{fc}M_{H_2}}{2F}$ for the instantaneous hydrogen consumption of the FC, as well as Equation (34) [28]. The results are shown in Table 7 below.

Table 7. Comparison of the results of each index before and after considering the depth of discharge of lithium batteries.

Indicator	Conventional Vessel Energy Management Strategy	Improved Vessel Energy Management Strategy
Hydrogen Consumption/g/day	3200	4032
Life Loss	2.9×10^{-3}	1.83×10^{-3}

As shown in Table 7, although the vessel consumes 832 g more hydrogen than the conventional energy management strategy when applying the improved energy management strategy, the lithium battery life loss is relatively reduced by 36.9%, which effectively extends the life of the lithium battery. Although the price of hydrogen will gradually decrease with the continuous improvement of hydrogen production technology in the future, the processing of lithium batteries is still a problem.

6. Conclusions

Considering the problem that the SOC equalization method used in the problem of the SOC imbalance of vessel energy storage equipment is likely to lead to the overcharging and discharging of energy storage equipment and early withdrawal from work, this paper proposes a distributed variable sag slope control strategy. This strategy can improve SOC equalization and the relation of functions between the dynamic compensation factor and SOC of energy storage equipment. This paper proposes an energy management strategy for a vessel hybrid power system, combining the operating mode switching strategy based on the supercapacitor’s SOC, the power allocation strategy with a variable filter time constant, and the energy management strategy for a hybrid FC vessel.

The simulation results show that the equalization speed and accuracy of the SOC of the vessel energy storage equipment are improved. The charging and discharging depths of the supercapacitors are reasonably controlled. The reasonableness of the output power distribution of different energy storage devices when the load power fluctuates is improved. The goals of achieving reasonable hydrogen consumption and a reduction in the life loss of energy storage equipment are attained.

Author Contributions: Conceptualization, Z.M., H.C., J.-F.C., M.B., and J.H.; methodology, H.C.; software, Z.M., Y.C.; validation, H.C., and Z.M.; writing—original draft preparation, Z.M.; writing—review and editing, H.C., J.-F.C., N.A.-A., J.H., M.B., and J.K.; visualization, Z.M.; supervision, H.C., J.-F.C., J.H., and M.B.; project administration, H.C.; funding acquisition, H.C. and M.B. All authors have read and agreed to the published version of the manuscript.

Funding: This research was supported by the Shanghai Science and Technology Commission project (Grant No. 20040501200), the Science Technology Commission of Shanghai Municipality, and the Shanghai Engineering Research Center of Ship Intelligent Maintenance and Energy Efficiency under Grant 20DZ2252300.

Institutional Review Board Statement: Not applicable.

Informed Consent Statement: Not applicable.

Data Availability Statement: The data that support the findings of this study are available within the article.

Conflicts of Interest: The authors declare no conflict of interest. The funders had no role in the design of the study; in the collection, analysis, or interpretation of data; in the writing of the manuscript, or in the decision to publish the results.

References

- Zhang, S.; Yuan, H. Overview of the 73rd Session of the Marine Environment Protection Committee of the International Maritime Organization. *World Shipp.* **2018**, *41*, 29–31.
- Pei, Z. Current situation and development trend of new energy power system for vessels. *Pop. Stand.* **2021**, *11*, 18–20.
- Sun, Y.; Hu, K.; Yan, X.; Tang, X.; Yuan, C. Review of Key Technical Issues of Hybrid Energy Storage System for New Energy Vessels. *Shipbuild. China* **2018**, *59*, 226–236.
- Yan, Q.; Mu, J.; Ma, Y.; Wang, Y.; Sun, Y. Overview of Distributed Energy Storage Application Model and Optimal Configuration. *Electr. Power Eng. Technol.* **2022**, *41*, 67–74.
- Mi, Y.; Cai, H.; Song, X.; Yu, S.; Li, Z. Charge State Equalization Study of Distributed Energy Storage Units Considering Mismatched Wire Resistance. *Proc. CSEE* **2019**, *39*, 4441–4451.
- Hoang, K.D.; Lee, H. Accurate power sharing with balanced battery state of charge in distributed DC microgrid. *IEEE Trans. Ind. Electron.* **2019**, *66*, 1883–1893. [[CrossRef](#)]
- Huang, X.; Xu, A.; Xu, D.; Yang, C.; Yang, F. Multi-intelligent distributed energy storage two-quadrant SOC consistent adaptive control. *China Sci.* **2019**, *14*, 1010–1014.
- Wang, X.; He, J.; Du, L. Decentralized control of series-parallel structure of DC microgrid battery energy storage system. *J. Power Supply* **2019**, *17*, 91–97.
- Lin, J.; Wang, Z.; Zhang, Y. Energy control strategies for distributed energy storage systems considering different capacities in independent DC microgrids. *Electr. Power Autom. Equip.* **2020**, *40*, 139–146.
- Lin, Y.; Xia, Y.; Wei, S. Plug-in Fuel Cell Electric Vehicle Energy Management Control Strategy Based on Augmented Learning Algorithm. *Chin. J. Eng.* **2019**, *41*, 1332–1341.
- Bassam, A.M.; Phillips, A.B.; Turnock, S.R.; Wilson, P.A. An improved energy management strategy for a hybrid fuel cell/battery passenger vessel. *Int. J. Hydrogen Energy* **2016**, *41*, 22453–22464. [[CrossRef](#)]
- Zhu, L.; Han, J.; Peng, D.; Wang, T.; Tang, T.; Charpentier, J.-F. Fuzzy logic based energy management strategy for a fuel cell/battery/ultra-capacitor hybrid ship. In Proceedings of the 2014 First International Conference on Green Energy ICGE 2014, Sfax, Tunisia, 25–27 March 2014; pp. 107–112.
- Zhang, Z. Study on Sizing and Energy Management Strategy of Hybrid Energy Storage for Hybrid Vessel. Master's Thesis, Wuhan University of Technology, Wuhan, China, 2019.
- Fang, S.; Wang, H.; Zhang, S.; Shang, C. Optimal ship energy storage system scheduling considering battery life loss. *Proc. CSEE* **2020**, *40*, 7566–7578.
- Zhao, Z. Improved fuzzy logic control-based energy management strategy for hybrid power system of FC/PV/battery/SC on tourist ship. *Int. J. Hydrogen Energy* **2022**, *47*, 9719–9734. [[CrossRef](#)]
- Guerrero, J.M.; Vasquez, J.C.; Matas, J.; de Vicuna, L.G.; Castilla, M. Hierarchical control of droop-controlled AC and DC microgrids—A general approach toward standardization. *IEEE Trans. Ind. Electron.* **2011**, *58*, 158–172. [[CrossRef](#)]
- Anand, S.; Fernandes, B.G.; Guerrero, J. Distributed control to ensure proportional load sharing and improve voltage regulation in low-voltage DC microgrids. *IEEE Trans. Power Electron.* **2013**, *28*, 1900–1913. [[CrossRef](#)]
- Tah, A.; Das, D. An enhanced droop control method for accurate load sharing and voltage improvement of isolated and interconnected DC microgrids. *IEEE Trans. Sustain. Energy* **2016**, *7*, 1194–1204. [[CrossRef](#)]
- Lin, X.; Zamora, R.; Baguley, C. A Fully Filter-Based Decentralized Control With State of Charge Balancing Strategy for Battery Energy Storage Systems in Autonomous DC Microgrid Applications. *IEEE Access* **2021**, *9*, 15028–15040. [[CrossRef](#)]

20. Li, P.; Zhang, C.; Yuan, R.; Kan, Z.; Chen, Y. Load Current Distribution Method for Distributed Energy Storage Systems with Improved SOC Sag Control. *Proc. CSEE* **2017**, *37*, 3746–3754.
21. Liu, Z.; Yang, C.; Jiang, W.; Li, P.; Yang, B. Power Allocation Technology for DC Microgrid Energy Storage System Based on Consistency Algorithm. *Autom. Electr. Power Syst.* **2020**, *44*, 61–69.
22. Shen, N.; Gao, J.; He, X. Research on a Scenery Power Smoothing Control Strategy Based on Hybrid Energy Storage System. *Electr. Energy Effic. Manag. Technol.* **2019**, *1*, 62–68.
23. Kannayeram, G.; Prakash, N.B.; Muniraj, R. Intelligent hybrid controller for power flow management of PV/battery/FC/SC system in smart grid applications. *Int. J. Hydrogen Energy* **2020**, *45*, 21779–21795. [[CrossRef](#)]
24. Sun, Y.; Xu, Q.; Yuan, Y.; Yang, B. Optimal Energy Management of Fuel Cell Hybrid Electric Vessels Considering Fuel Cell Aging Cost. In Proceedings of the 2020 IEEE/IAS Industrial and Commercial Power System Asia, Weihai, China, 13–16 July 2020; pp. 240–245.
25. Yang, W.; Liu, X. Multi-objective Genetic Algorithm Based Configuration Optimization of Shipboard Energy Storage System. *Electron. Meas. Technol.* **2021**, *44*, 49–53.
26. Li, X.; Ma, R. Energy Management Method for Energy Storage Systems Considering Battery Pack Health Status. *Power Syst. Technol.* **2020**, *44*, 4210–4217.
27. Banaei, M.; Rafiei, M.; Boudjadar, J.; Khooban, M.H. A Comparative Analysis of Optimal Operation Scenarios in Hybrid Emission-Free Ferry Vessels. *IEEE Trans. Transp. Electrification* **2020**, *6*, 318–333. [[CrossRef](#)]
28. Liu, Q.; Zhan, Y.; Li, R. Multi-objective Optimization of Energy Management Strategy for Fuel Cell Vehicles. *Electron. Meas. Technol.* **2020**, *43*, 31–36.

Disclaimer/Publisher’s Note: The statements, opinions and data contained in all publications are solely those of the individual author(s) and contributor(s) and not of MDPI and/or the editor(s). MDPI and/or the editor(s) disclaim responsibility for any injury to people or property resulting from any ideas, methods, instructions or products referred to in the content.